Dalton Transactions

Accepted Manuscript

ROYAL SOCIETY OF CHEMISTRY

www.rsc.org/dalton

Dalton Transactions

Dynamic Article Links ▶

Cite this: DOI: 10.1039/c0xx00000x

www.rsc.org/xxxxxx

COMMUNICATION

Black and Yellow Anatase Titania Formed by (H,N)-doping: Strong Visible-light Absorption and Enhanced Visible-light photocatalysis

Shunhang Wei, Rong Wu*, Jikang Jian, Fengjuan Chen and Yanfei Sun

Received (in XXX, XXX) Xth XXXXXXXXX 20XX, Accepted Xth XXXXXXXXX 20XX

DOI: 10.1039/b000000x

We produce black and yellow anatase TiO_2 doped with hydrogen and nitrogen elements annealing in N_2/Ar/air atmosphere. More interestingly, one kind of black TiO_2 has excellent performance for degradation of methylene blue under visible-light irradiation but photodegradation of the other one is quite limited.

Titanium dioxide (TiO_2) has emerged as the most widely investigated photocatalyst for using in solar-driven clean energy.[1] The photocatalytic process is carried out through the activation of a semiconductor material with UV or visible light illumination.[2] Thus high effective light absorption is essential to maximize photocatalytic performance. However, conventional white TiO_2 has poor visible absorption because of a wide band gap (3.2eV for anatase).[3] Also, the rapid electron-hole recombination of TiO_2 often results in poor photocatalytic activity. Many methods to prepare TiO_2-based photocatalysts that enable efficient utilization of visible light have been developed. A frequently used method is doping TiO2 with metals or nonmetals such as Ag[4], Mo[5], N[6], C[7]. Nevertheless, the above two major issues affecting the efficiency of light absorption and photocatalysis have not been well resolved. Recently, hydrogenation has been used to produce black TiO_2 to improve visible light absorption and photocatalytic activity, which has attracted extensive attention.[8] Indeed, Chen *et al.*[8] have shown that black TiO_2 produced by hydrogenation can have a narrow band gap of 1.54eV, which improves visible and infrared optical absorption. However, the visible-light photocatalytic activity of this sample was not very high.[9-12]

To date, four methods have mainly been used to produce black TiO_2, including (1) high H_2-pressure process[8], (2) annealing in hydrogen atmosphere[13], (3) aluminum reduction[14] and (4) solution evaporation process[15]. Method (1) is dangerous because it is difficult to control a hydrogenation process conducted at high pressure (20bar) using pure hydrogen. Through methods (2) and (3) possess well photocatalysis performance under visible-light illumination, the appearance of hydrogen also makes these experimental processes unsafe. Method (4) is a safer option, which synthesizes black anatase titania without hydrogenation, and provide a new path for the preparation of black TiO_2. However, the existing approach is troublesome to handle. The major reasons are that $TiCl_4$ as experimental material is easy volatile so that need operational process making under ice water bath and produce corrosive gas when it meet water. Therefore, a safer and more simple synthesis method is required to produce black titania with excellent photocatalytic activity.

Herein, a new facile synthetic method to produce black TiO_{2-x} is developed by chemical synthetic approach. In this method, tetrabutyl titanate is used as a titanium precursor and the equipments used before calcined are very simple: a heat-preservation device and magnetic stirrer. The synthesized black TiO_{2-x} sample exhibits excellent visible-light absorption, which highly increases photocatalytic activity. In this process, yellow TiO_2 with good performance can also be produced using different heating environment.

The X-ray diffraction (XRD) patterns of the TiO_2 samples annealed under different gases are presented in Fig. 1a: black TiO_2 heated in Ar atmosphere (B(Ar)), black TiO_2 heated in N_2 atmosphere (B(N_2)), yellow TiO_2 heated in air (Y(air)). The patterns are all consistent with anatase TiO_2. The intense XRD diffraction peaks indicate that the yellow and black TiO_2 samples are highly crystalline. The structural characteristics of the three samples were further investigated by Raman spectroscopy, as shown in Figure 1b. Anatase TiO_2 has six Raman-active modes at 144, 197, 399, 515, 519 (superimposed with the 515 cm^{-1} band), and 639 cm^{-1}, respectively.[1] Therefore, the Raman spectra unambiguously indicate that all of these samples are typical anatase TiO_2. Compared with yellow TiO_2, the most intense peak at 144 cm^{-1} of the two black TiO_2 samples exhibits a blue shift, which is ascribed to the crystal domain size and nonstoichiometry.[14]

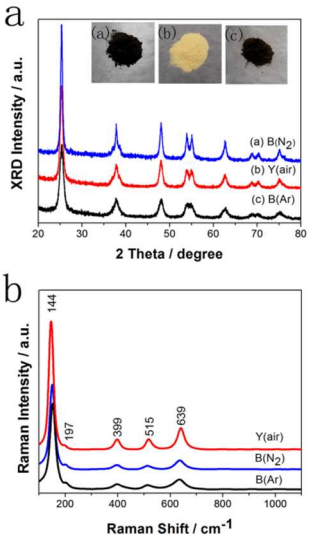

Fig. 1 XRD patterns (a) and Raman spectra (b) of black TiO_2 calcined in N_2 (B(N2)), yellow TiO_2 calcined in air (Y(air)) and black TiO_2 calcined in Ar (B(Ar)).

X-ray photoelectron spectroscopy (XPS) is used to detect the surface chemical bonding and valence state of samples. The spectra in Fig. 2b and c indicate that there are trivalent and

tetravalent Ti on the outermost surface of the black anatase TiO_2. The related binding energies are 457.6 and 458.5 eV for the sample annealed in Ar, respectively, and 458.4 and 458.7 eV for that annealed in N_2, respectively (see Fig.1S for more details in the ESI†). The proportion of trivalent to tetravalent Ti in B(Ar) is calculated to be 1/24.85 from the peak areas for the outermost surface, while that for $B(N_2)$ is 1/18.20. Therefore, B(Ar) and $B(N_2)$ are assumed to possess stoichiometries of $TiO_{1.980}$ and $TiO_{1.974}$ for the outermost surface, respectively. The presence of Ti^{3+} in the samples is further supported by electron paramagnetic resonance (EPR). A strong EPR signal observed at g-value of ~2.002 is assigned to surface Ti^{3+} (Fig.2S in the ESI†).[16] Given that the signal area is correlated with the amount of Ti^{3+}, it indicates that the largest amount of Ti^{3+} and oxygen vacancies exist in $B(N_2)$ samples. In contrast, Ti^{3+} is not present in the yellow TiO_2 (Fig. 2a and Fig.2S). In other words, there are fewer oxygen vacancies in the yellow TiO_2 sample than in the black ones. To the outermost surface, oxygen deficiency ratios of 0.02 and 0.05 exceed 0.01 too much, which result in anatase TiO_2 undergoing phase transformation.[17] However, the results of XRD (Fig. 1a) and Raman spectroscopy (Fig. 1b) demonstrated that the samples are typical anatase TiO_2. A similar inconsistency was also reported by Myung *et al*.[15] Based on above results, such apparent contradiction can be ascribed to the introduction of N and H during high-temperature annealing. Forms of being of N and H in samples are reflected by the N 1s XPS spectrum (Fig.3S in the ESI†). The broad peak of $B(N_2)$ can be deconvoluted into two peaks, while that for B(Ar) is three peaks. The peaks of $B(N_2)$ centered at 400.1eV and 399.2eV and the peak of B(Ar) and Y(air) centered at 399.8eV and 402.1eV can be ascribed to amines (NH_x) respectively.[3,18] The peaks of Y(air) at 396eV is attributed to Ti-N-Ti bond.[19] The synthetic peak of B(Ar) centered at 397.2eV agrees with the binding energy of N in oxynitride (O-Ti-N) bonding.[18] The peak centered at 401.4eV is ascribed to NH_3^+ or NH_4^+. The absence of this peak in $B(N_2)$ shows the absence of NH_3^+ or NH_4^+ or only very little amount of them. Given that the temperature of nitrogen element from the decomposition of N_2 gas doping into TiO_2 need more than 700□ under annealed in only N_2 gas,[20] the presence of N and H in our samples is attributed to the use of urea as a reductant, and allow the anatase titania structure maintained.

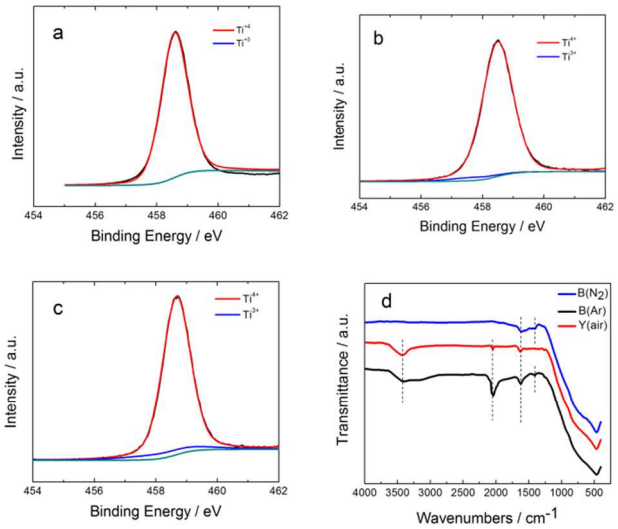

Fig. 2 XPS obtained for (a) Y(air), (b) B(Ar), and (c) $B(N_2)$. (d) FTIR spectra of the three TiO_2 samples.

FTIR spectra of the black and yellow anatase TiO_2 samples are illustrated in Fig. 2d. The peaks at around 3400 and 1620 cm^{-1} are attributed to stretching and bending vibrations of hydroxyl groups, respectively.[21] The peak at around 2000 cm^{-1} is attributed to stretching and bending vibrations of NH_3^+. An additional peak at 1390 cm^{-1} is found for black anatase TiO_2 that can be assigned to the bending vibration of NH_4^+.[22] Interestingly, the peak at around 2000 cm^{-1} is not present in the FTIR spectrum of $B(N_2)$. This is mainly because the furnace used to calcine $B(N_2)$ possessed better gas tightness than that used to calcine the other samples, so ammonium was decomposed more entirely during heat treatment. The FTIR spectra are consistent with the presence of N and H in the samples. At the same time, the results of FTIR demonstrate the peak of B(Ar) centered at 401.4eV is ascribed to the coexistence of NH_3^+ and NH_4^+ rather than one of them and the absence of the peak at around 401eV in $B(N_2)$ is attributed to very little amount of NH_4^+ or NH_3^+ rather than its absence. Time-of-flight secondary ion mass spectroscopy (ToF-SIMS) is employed to further demonstrate our assumption. The results show that NH_3^+ (m=17) and NH_4^+ (m=18) do exist in two black samples (Fig.3S in the ESI†). Based on this result, besides very little amounts of them exist in $B(N_2)$, the absent FTIR peak of NH_3^+ in $B(N_2)$ show the amounts of NH_3^+ less than NH_4^+. It is consistent with the deduction that ammonium decomposition more entirely. None carbon-related fragments are detected, such as C^+ (m=12), C_2^+ (m=24) and C_2H^+ (m=25) (Fig.4S in the ESI†).[15] Therefore, the ToF-SIMS date demonstrate two black TiO_2 are carbon-free samples.

Comparing Fig. 2a with b and c, we note the absence of trivalent Ti in the yellow anatase TiO_2. However, the FTIR spectrum of Y(air) shows that N and H are also doped in yellow anatase TiO_2. It is assumed that during heat treatment, the oxygen present in air makes it difficult for ammonium to enter TiO_2, the following decomposition can not go on entirely and finally make the formation of NH_3^+ . The presence of oxygen decreasing the amounts of N and H doped into TiO_2 makes the reduction of tetravalent Ti unsuccessful. This assumption is consistent with the above deduction that good gas tightness with less oxygen present during heat treatment improves doping with N and H and entirely decomposition of ammonium.

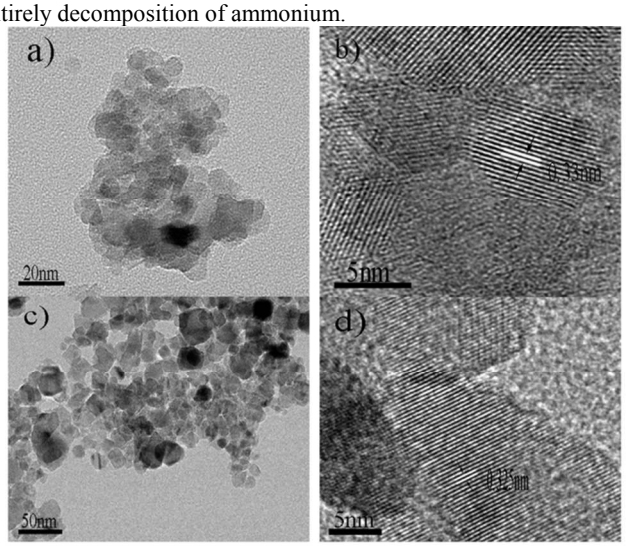

Fig. 3 (a) TEM image of black anatase TiO_2 (Ar). (b) HRTEM micrographs of black anatase TiO_2 (Ar). (c) TEM image of black anatase TiO_2 (N_2). (d) HRTEM micrographs of black anatase TiO_2 (N_2).

Transmission electron microscopy (TEM) was used to investigate the morphology and particle size of the synthesized powders. Fig. 3a and c reveal that the average diameter of the nanocrystals are ~8.2 nm for B(Ar) and ~26 nm for $B(N_2)$. High-resolution transmission electron microscopy (HRTEM) was used

to examine the microstructure of the black anatase TiO_2 samples, as shown in Fig. 3b and d. These images indicate that the distance in the crystal lattices are ~0.33 and ~0.325 nm, consistent with (101) lattice planes. The surface of two black samples also show the absence of carbon layers. The sample heated in Ar atmosphere is very black before milling with an agate mortar. After milling, a small amount of the sample appears dark green. This phenomenon is attributed to the diameter of the nanocrystals being decreased by milling, which changes the refractive index of the sample.

Annealing in air, Ar or N_2 controlled whether yellow or black TiO_2 was obtained. The different colors indicate that these samples possess different light-absorption properties. Fig. 4a shows UV-vis spectra of the black and yellow anatase TiO_2 samples. The black samples absorb visible light much more strongly than the yellow sample, and black TiO_2 (N_2) absorbs visible light better than black TiO_2 (Ar). In addition, the yellow samples absorb visible light better than P25 (a mixture of anatase and rutile) which is nearly no absorbance in visible light.

The band-gap energies of the samples were calculated from their absorbance spectra by assuming a direct transition in the anatase TiO_2 crystal from $(Ah\nu)^2$ versus $h\nu$, where A is absorbance, h is Planck's constant, and ν is the frequency of light.[23] The band-gap energies of the samples are presented in Fig. 4b. The band gap energy of the yellow sample is 2.5 eV, which is considerably smaller than that of typical TiO_2 (3.2 eV). The difference is assumed to be associated with the small number of doped H and N atoms. The band-gap energies of B(Ar) and B(N_2) are 2.0 and 1.5 eV, respectively. Apparently, the presence of Ti^{3+} and doped elements N and H narrow the band gap of black TiO_2.

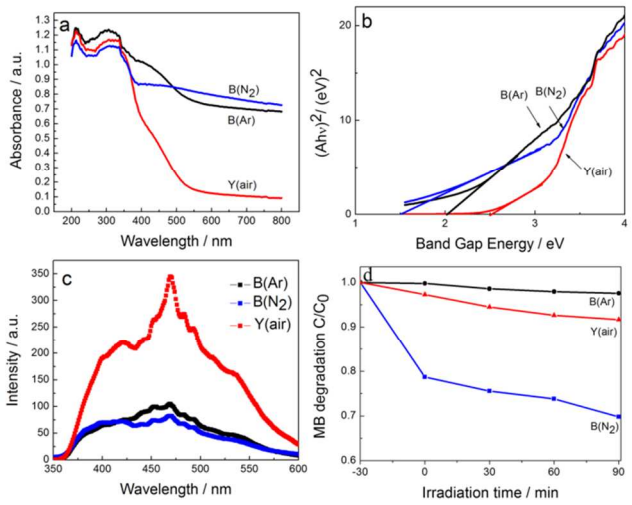

Fig. 4 (a) Spectral absorbance of the yellow TiO_2 (Y(air)) and the black TiO_2 calcined in Ar (B(Ar)) and N_2 (B(N_2)). (b) Band-gap energies of three samples (c) PL emission spectra of samples (d) Visible-light photocatalytic degradation of methylene blue (MB) by various samples

The photoluminescence emission spectroscopy (PL) emission spectroscopy has been widely used to determine the effectiveness of charge carrier trapping, migration and transfer of charge carriers, and understand the fate of electron/hole pairs in semiconductors because PL emission results from the recombination of free carriers.[24,25] Fig. 4c shows the PL spectra of the yellow TiO_2 and black TiO_{2-x} samples in the wavelength range of 350–600 nm following excitation at 300 nm. The first peak at 400 nm (3.2 eV) is attributed to the emission from the band-gap transition. The second peak at 420 nm is ascribed to band-edge free excitons, while the other two peaks at 482 and 493 nm are attributed to bound excitons.[24,26] The main PL emission peaks of three samples appear at 451 and 469 nm, which are attributed to surface oxygen vacancies and defects of TiO_2 samples.[25] The intensitive peak at 469 nm reaching the summit demonstrate the formation of oxygen defects in all the three samples.[9] Some other peaks observed in the PL spectra may result from surface defects present in the samples.[27] The intensity of the PL spectra show a significant decrease due to the presence of Ti^{3+} and vast oxygen vacancies. The reduction of PL intensity indicates that B(N_2) and B(Ar) have a relatively low recombination rate of electron/hole pairs compared with that in Y(air). This is because that the traps resulting from surface defects and oxygen vacancies affect the movement and distribution of electron/hole pairs, impeding their recombination.

Given that the adsorption of organic molecules to the titania surface is a pivotal step in photocatalytic degradation, it is essential to investigate the adsorption characteristics of MB onto the surface of the different samples. Obviously, after equilibrium in the dark for 30 min, most dye molecules remain in the solution with B(Ar) and Y(air) as the catalyst, whereas a large amount of dye molecules (ca. 21.3%) is adsorbed on the surface of B(N_2) sample (see Table 1S in ESI†).The photocatalytic decomposition of MB by the samples under visible-light illumination was investigated; the results are presented in Fig. 4d. The black TiO_2 annealed in N_2 exhibits higher photocatalytic activity than the other two samples. For B(N_2), the degradation of MB reaches 30.2% after irradiation for 90 minutes with visible light. In contrast, Y(air) only decomposes about 8.3% of MB within 90 minutes, while B(Ar) barely degrades MB. It is well known that a high spectral response range and low photogenerated carrier recombination rate result in excellent photocatalytic activity. The introduction of Ti^{3+}, numbers of oxygen vacancies and surface defects layer make both B(N_2) and B(Ar) with these properties. And the different performance between B(N_2) and Y(air) also demonstrate the result. It is unexpected that B(Ar) contains such species but has quite limited photocatalytic activity. According to our knowledge, such discovery on anatase titania has not been reported before, so we decided to investigate the reason behind it.

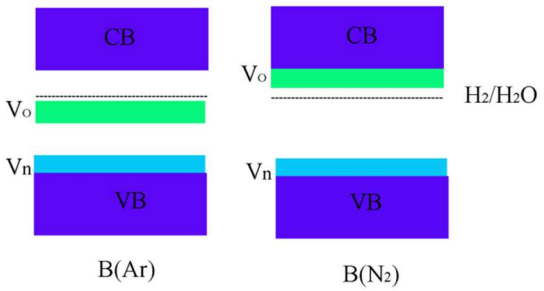

Fig. 5 Schematic diagrams of the band structures of black TiO_2 samples

The difference of the electronic structure of black TiO_2 crystals are clearly seen upon comparing the UV-visible absorption spectra of B(N_2) and B(Ar). As shown in Fig. 4a, an absorption valley at 386nm （3.2eV) indicates an unchanged intrinsic bandgap. However, owing to the appearance of vast oxygen vacancy, oxygen vacancy band (Vo) making the transition of electron from valance band more easy is induced, which is the reason that the bandgap of them is narrowed to about 1.5eV and 2.0eV, respectively. Interestingly, an additional visible light absorption band with an edge extending to around 600nm (2.0eV) is observed for B(Ar) but not B(N_2). In order to further understand this phenomenon in our black titania samples, the

mechanism of band structures of B(Ar) and B(N_2) in our experiment is schematically illustrated in Fig. 5. The substitutional nonmental doping of N and H , especially the *p* states of N contribute to the band-gap narrowing by mixing with O 2*p* states, make the formation of new valence band (Vn).[3] The formation of a visible-light absorption band is ascribed to Vo, which lies below conduction band minimum. Based on the date of XPS, FTIR and ToF-SIMS, it is deduced that the presence of more amount of NH_3^+ leads to this phenomenon. Theoretical work suggested that the high enough concentration of Ti^{3+} can induce a continuous vacancy band of electronic states just below the conduction band edge of TiO_2, while a low Ti^{3+} doping concentration only creates localized oxygen vacancy states that actually reduce the electron mobility and exhibit a negligible visible photoactivity.[28,29,30] Hence, Vo in B(N_2) exist just below the conduction band due to high concentration of Ti^{3+}, which also supported by the absence of other visible-light absorption bands. The reason that B(Ar) shows poor photocatalytic activity can be deduced that the presence of more amount of NH_3^+ impedes the vacancy-induced band of electronic states closing to conduction band and the formation of lots of Ti^{3+} so that the location of oxygen vacancy-induced band (Vo) lies below the H_2/H_2O redox potential.[28,31] In addition, NH_3^+ is also present in Y(air), but Y(air) performs better than B(Ar). It can be assumed that the amount of NH_3^+ in B(Ar) is greater that in Y(air). Less existence of NH_3^+ results in better photocatalytic degradation performance. Therefore, our results indicate that the excellent photocatalytic performance of B(N_2) can ascribed to two factors: (1) the presence of Ti^{3+}, which increases the number of oxygen vacancies, leading to the formation of an oxygen vacancy-induced band; (2) the presence of less NH_3^+, which benefits to the oxygen vacancy-induced band closing to conduction bands.

Conclusions

In summary, the present work demonstrates a new chemical approach to prepare black anatase TiO_{2-x} and yellow anatase TiO_2 nanoparticles by doping with N and H. The introduction of trivalent Ti and numerous oxygen vacancies strongly enhances visible-light absorption and the photocatalytic performance of the catalysts under visible light. The band-gap energy of the samples is also decreased substantially. By comparing the performance of three samples, we found that the appearance of more amount of NH_3^+ can be attributed to inferior gas tightness during annealing and limits photocatalytic activity because it causes V_O to lie below the H_2/H_2O redox potential. We developed a simple, safe method to prepare black anatase titania with excellent absorption and photocatalytic performance. This method may provide a new way to improve TiO_2 photocatalysis for water cleaning applications.

Notes and references

This work was financially supported by the National Natural Science Foundation of China (No.11164026)

Key Laboratory of Solid-state Physics and Devices, School of Physical Science and Technology, Xinjiang University ,Urumqi830046,China. Email: wurongxju@sina.com

† Electronic Supplementary Information (ESI) available: Experimental details / EPR / XPS / ToF-SIMS. See DOI: 10.1039/c000000x/

1 X. Chen, S. S. Mao, *Chem. Rev.* 2007, 107, 2891.
2 A. Alinsafi, F. Evenou, E. M. Abdulkarim, M. N. Pons, O.Zahraa, A. Benhammou, A. Yaacoubi, A. Nejmeddine, *Dyes Pigm* 2007, 74, 439.
3 R. Asahi, T. Morikawa, T. Ohwaki, K. Aoki, Y. Taga, *Science* 2001, 293, 269.
4 C. Y. Su, L. Liu, M. Y. Zhang, Y. Zhang, C. L. Shao, *CrystEngComm* 2012, 14, 3989.
5 L. G. Devi, B. N. Murthy, *Catal. Lett.* 2008, 125, 320.
6 J. Wang, C. Y. Fan, Z. M. Ren, X. X. Fu, G. D. Qian, Z. Y. Wang, *Dalton Trans.* 2014, 43, 13783.
7. H. Y. Li, D. J. Wang, H. M. Fan, P. Wang, T. F. Jiang, T. F. Xie, *J. Colloid Interface Sci.* 2011, 354, 175.
8 X. B. Chen, L. Liu, P. Y. Yu, S. S. Mao, *Science* 2011, 331, 746.
9 X. D. Jiang, Y. P. Zhang, J. Jiang, Y. S. Rong, Y. C. Wang, Y. C. Wu, C. X. Pan, *J. Phys. Chem.C* 2012, 116, 22619.
10 A. Naldoni, M. Allieta, S. Santangelo, M. Marelli, F. Fabbri, S. Cappelli, C. L. Bianchi, R. Psaro, V. Dal Santo, *J. Am.Chem. Soc.* 2012, 134, 7600.
11 Z. K. Zheng, B. B. Huang, J. B. Lu, Z. Y. Wang, X. Y. Qin, X. Y. Zhang, Y. Dai, M. H. Whangbo, *Chem. Commun.* 2012, 48, 5733.
12 J. H. Park, S. Kim, A. J. Bard, *Nano Lett.* 2006, 6, 24.
13 G. M. Wang, H. Y. Wang, Y. C. Ling, Y. C. Tang, X. Y. Yang, R. C. Fitzmorris, C. C. Wang, J. Z. Zhang, Y. Li, *Nano Lett.* 2011, 11, 3026.
14 Z. Wang, C. Y. Yang, T. Q. Lin, H. Yin, P. Chen, D. Y. Wan, F. F. Xu, F. Q. Huang, J. H. Lin, X. M. Xie, M. H. Jiang, *Energy Environ. Sci.* 2013, 6, 3007.
15 S. T. Myung, M. Kikuchi, C. S. Yoon, H. Yashiro, S. J. Kim, Y. K. Sun, B. Scrosati, *Energy Environ. Sci.* 2013, 6, 2609.
16 A. L. Attwood, D. M. Murphy, J. L. Edwards, T. A. Egerton, R. W. Harrison, *Res Chem Intermed.* 2003, 29, 449
17 K. Szot, M. Rogala, W. Speier, Z. Klusek, A. Besmehn, R. Waser, *Nanotechnology* 2011, 22 (25).
18 J. Hensel, G. Wang, Y. Li, J. Z. Zhang, *Nano Lett.* 2010,10,478.
19 X. L. Guo, J. Dai, K. Zhang, X. D. Wang, Z. Cui, J. Y. Xiang, *Textile Research Journal* 2014, 84: 1891.
20 Y. F. Ju, X. T. Zu, X. Xiang, *High Power Laser and Particle Beams* 2008, 20(1):0143.
21 J. Fang, F. C. Shi, J. Bu, J. J. Ding, S. T. Xu, J. Bao, Y. S. Ma, Z. Q. Jiang, W. P. Zhang, C. Gao, W. X. Huang, *J. Phys. Chem. C* 2010, 114, 7940.
22 K.M.S. Khalil, M.I. Zaki, *Powder Technol.* 1997, 92, 233.
23 D. J. Park, T. Sekino, S. Tsukuda, S. I. Tanaka, *Res Chem Intermed.* 2013, 39, 1581.
24 L. Q. Jing, Y. C. Qu, B. Q. Wang, S. D. Li, B. J. Jiang, L. B. Yang, W. Fu, H. G. Fu, J. Z. Sun, *Sol. Energy Mater. Sol. Cells* 2006, 90, 1773.
25 Q. J. Xiang, K. L. Lv, J. G. Yu, *Appl. Catal. B* 2010, 96, 557.
26 J. G. Yu, L. Yue, S. W. Liu, B. B. Huang, X. Y. Zhang, *J. Colloid Interface Sci.* 2009, 334, 58.
27 G. L. Zhu, T. Q. Lin, X. J. Lu, W. Zhao, C. Y. Yang, Z. Wang, H. Yin, Z. Q. Liu, F. Q. Huang, J. H. Lin, *J. Mater. Chem. A* 2013, 1, 9650.
28 I. Justicia, P. Ordejon, G. Canto, J. L. Mozos, J. Fraxedas, G. A. Battiston, R. Gerbasi, A. Figueras, *Adv.Mater.* 2002, 14, 1399.
29 G. R. Torres, T. Lindgren, J. Lu, C. G. Granqvist, S. E. Lindquist, *J. Phys. Chem. B* 2004, 108, 5995.
30 X. Liu, S. M. Gao, H. Xu, Z. Z. Lou, W. J. Wang, B. B. Huang, Y, Dai, *Nanoscale* 2013, 5, 1870.
31 D.C. Cronemeyer, *Phys. Rev.* 1959, 113,1222.